Hindawi
Geofluids
Volume 2022, Article ID 7984910, 13 pages
https://doi.org/10.1155/2022/7984910

Research Article

Analysis Deformation Failure Characteristics and the Energy Evolution of Varying Lithologies under Cyclic Loading

Jianqiang Liu[1,2] **Guangpeng Qin**[1,2,3] **Jing Cao**[4] **and Minghua Zhai**[3]

[1]*College of Resource, Shandong University of Science and Technology, Tai'an, Shandong 271000, China*
[2]*National Engineering Laboratory for Coalmine Backfilling Mining, Shandong University of Science and Technology, Tai'an, Shandong 271000, China*
[3]*Shandong Energy Group Co., Ltd., Ji'nan, Shandong 250100, China*
[4]*College of Finance and Economics, Shandong University of Science and Technology, Tai'an, Shandong 271000, China*

Correspondence should be addressed to Guangpeng Qin; skd992807@sdust.edu.cn and Jing Cao; skd993798@sdust.edu.cn

Received 22 March 2022; Revised 16 May 2022; Accepted 17 May 2022; Published 6 June 2022

Academic Editor: Yong-Zheng Wu

Deep underground engineering often utilizes cyclic loading. To understand the deformation and damage characteristics of rock under cyclic loading conditions, cyclic loading tests of three different specimens with varying lithology were performed. The dissipated energy method was used to analyze the magnitude of damage and rock failure characteristics during the energy evolution process of cube specimens. The results indicated that the modulus of elasticity of three lithologies were stable prior and subsequent to cyclic loading. While the cyclic loading profile improved the rock's resistance to deformation, it increased the internal mesostructure defects. Rock damage caused by the cyclic loading reduced the uniaxial compression strength. This was especially true for coal samples. For coal samples, these observations were consistent with internal coal damage calculated by analysis. Under the same lithology and different loading modes, rock damage was caused by cyclic action, and the elastic strain energy released by instantaneous unloading of rock samples with significant damage was reduced. The rupture magnitude for cyclic loading was observed to be less than that of uniaxial compression. Under cyclic loading and varying different lithologies, sandstone absorbed the most energy, resulting in a larger final fracture magnitude compared to other lithologies.

1. Introduction

With the acceleration of industrialization, near-surface resources are being gradually exhausted, and the development and utilization of deep mineral resources has become essential [1]. Due to the significant depth to access deep mineral resources, roadways to access such resources are surrounded by rock in a variable geological environment. The presence of the tunnel containing the roadway has a direct impact on the stability of the surrounding rock. This is consequence of the tunnel's structural characteristics, the strength and mechanical properties of the surrounding rock, and the impact of excavation unloading. In addition, related support disturbance, propagating up to three support heights into surrounding rock, is a key factor for the deformation and failure of rock surrounding a deep tunnel [2, 3, 4]. In the engineering activities such as deep coal mining, the excavation of roadway tunnels was processed with forward excavation support, chamber, and tunnel excavation. During these processes, the surrounding rock experiences cyclic loading and unloading. The cyclic load will cause the mechanical properties of the surrounding rock to deteriorate and induce secondary failures. Such processes are more serious for deep roadway excavation.

Scholars globally have characterized the stress and energy evolution under cyclical loading conditions. In addition, damage characteristics have also been characterized. Research in these area includes Meifeng et al. [5], Li et al. [6], and Wu et al. [7]. From the perspective of thermodynamics, instable rock destruction is the factor driving energy conversion, accumulation, dissipation, and other similar processes. There is a connection between the expansion

and development of rock internal microcracks, energy evolution law, and destructive morphology. Consequently, there is important theoretical significance to characterizing the destructive rock behavior from the perspective of energy evolution. Based on damage mechanics, Lei et al. [8] established a shear damage evolution model for joints which considered freeze-thaw cycles and joint persistence. Kai-Nan et al. [9] conducted Brazil splitting tests for shale and characterized the sample energy distribution characteristics. Yao and Wang [10] studied the energy variation rule for granite experiencing uniaxial compression failure and concluded that there was a linear relationship between energy and confining pressure in the failure process. Li et al. [11] conducted compression tests for coal at different loading rates and studied the relationship between energy conversion of coal and lumpiness after crushing. Ping et al. [12] conducted compression damage experiments on white sandstone under uniaxial conditions with different loading rates along with triaxial loading experiments with varying confining pressures and different control modes. In addition, Li et al. [11] discussed the relationship between the loading rate and both the final failure form and the ultimate strength of white sandstone. Loading rate was also related to confining pressure, loading control, and unloading control. Meng et al. [13] performed uniaxial compression tests on red sandstone with varying sizes and strain rates. It was found that the higher the absorption energy of red sandstone, per unit volume, in the compression process, the larger the magnitude of the final rupture. Liu et al. [14], Xu et al. [15], and Zhizhen and Feng [16] conducted cyclic loading tests under uniaxial compression for sandstone, characterized the relationship between load and elastic energy and dissipated energy, and analyzed sandstone rock burst propensity using the elastic energy index. Li et al. [17] calculated a preliminary estimate of the spatter velocity of broken rock particles based on the principle of energy conservation and provided a set of steps and methods for preliminary analysis of the overall failure mode together with the state and strength of rock mass structure from the perspective of an energy budget. Guo et al. [18] studied the mechanical properties and deformation characteristics of rock under uniaxial cyclic loading and characterized the stress-strain curve under each cyclic loading. The stress-strain curve formed a hysteresis loop which translated in the direction of increasing strain. Yang et al. [19] conducted uniaxial and cyclic tests on a coal-rock assemblage and found that dissipative energy accumulated had experienced sudden changes. In addition, it was indicated that rock fracture is caused by the release of elastic strain energy. Liu et al. [20] and Cheng and Xiao [21] used normalized dissipative energy to characterize rock damage. Zhang et al. [22–23] studied the fragmentation process of granite through acoustic emission observations and studied the law of total elastic strain energy change at different times. In addition, acoustic emission events under different stress conditions were studied. In addition, research regarding rock damage has also been a research topic receiving considerable attention. Chuang et al. [24] established damage variable expression based on residual strain principles and Yang et al. [25] established damage variable expression based on energy principles. Residual deformation accumulation is an external manifestation of internal damage. It is a qualitative rather than quantitative indicator. Energy is the internal cause of driving damage. The damage model based on energy principles may objectively reflect the damage evolution during rock deformation. In terms of rock uniaxial compression, Zhao et al. [26] conducted quasistatic and dynamic uniaxial compression tests on cylindrical thick-walled granite specimen with different clay filling volumes to understand the dynamic characteristics of rock in a mud-water environment. Fan et al. [27] conducted uniaxial compression tests on samples with a single nonpenetrating defect and presented the crack growth behavior and fracture characteristics of sandstone specimens with nonpenetrating fractures during uniaxial loading.

Most of the mentioned studies were based on the loading of rocks or with lower limit stresses, which did not fully reflect the cumulative effect of energy-induced fatigue damage and the nature of the rock damage processes. Based on this study's context, utilizing the rock destruction theory of energy change, the load cycle addition and unloading of different rock tests are developed to provide a theoretical basis for geotechnical engineering practice.

2. Materials and Methods

2.1. Engineering Background. Shandong Energy Zaozhuang Mining Group's Fucun Mine 1009 contains a working surface material roadway which utilizes tunnel arm excavation after the use of anchor parallel operation technology. The parallel operation of the tunnel construction area is divided into a header cutting area and an anchor operation area. The front of the header and the header behind the anchor operation division operate in parallel. The working area contains the roadway hydraulic support, back circulation support, and hydraulic door support. The working principle utilizes auxiliary support lifting the front of the manipulator roadway door hydraulic support from the support area. This support method is equivalent to a roof. Such an area which contains two cycle loading effects may cause surrounding rock strength deterioration and induce secondary failures. This risk is suggested by the working principle utilized by door hydraulic support and the indoor tests of loading and unloading. See Table 1 for material lithologic characteristics of the 1009 working face and see Figure 1 for hydraulic portal support.

Verification of the effectiveness of the hydraulic temporary support for improving stability of the rock surrounding the new roadway tunnel is vital. Also, characterizing the deformation and failure characteristics of rock surrounding the roadway when subjected to the installation of an advanced temporary support structure is very important for fast and safe roadway excavation. According to the actual geological situation of the roadway surrounding rock and the working principle of hydraulic portal support, cyclic loading and unloading tests related to sandstone, mudstone, and coal are carried out, combined with uniaxial compression test, to analyze the deformation and damage

Table 1: Comprehensive histogram of working face conditions.

No.	Thickness (m)	Depth (m)	Formation	No.	Thickness (m)	Depth (m)	Formation
1	1.85	52.66	Medium sandstone	6	5.5	82.46	Coal seam
2	9.0	61.66	Fine sandstone	7	0.3	82.76	Mudstone
3	10	71.66	Medium sandstone	8	5.12	87.88	Siltstone
4	5	76.66	Siltstone	9	0.15	88.03	Sandy mudstone
5	0.3	76.96	Mudstone				

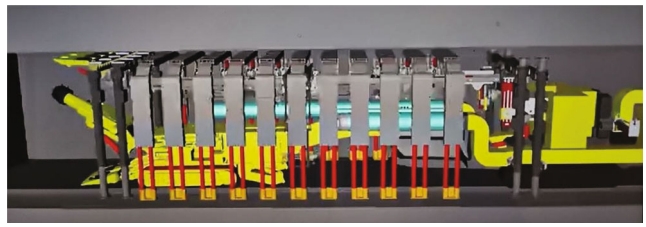

(a)

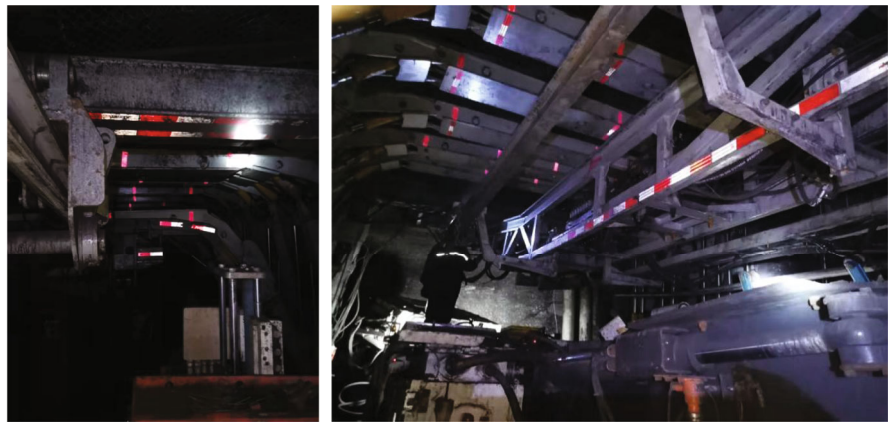

(b)

Figure 1: Hydraulic door bracket. (a) Renderings of hydraulic door-type bracket. (b) Photo of the hydraulic gate bracket.

characteristics and energy evolution law of the roadway surrounding rock.

2.2. Test Process

2.2.1. Sample Preparation. The large coal block and roof slab rock block were collected at the site and analyzed in the laboratory. During this analysis, three rock samples including sandstone, mudstone, and coal were utilized. These samples characterized the site lithological conditions. After cutting, grinding, and processing into a standard $70 \times 70 \times 70$ mm sample, the flatness and verticality of the processed test sample were verified to satisfy the rock test specification standard. The equipment used included a cutter (DQ-6) and grinder (SHM-200) shown in Figure 2(a), while the resulting sample is shown in Figure 2(b).

2.2.2. Test Scheme. Specimen combinations including rock, sandstone, mudstone, and coal were used and analyzed. Prior to cyclic loading, an uniaxial compression test was conducted on each lithology sample. In order to minimize measurement error, three samples were selected for duplicate testing test to determine the average compressive strength of varying lithologies. In addition, to magnify the failure characteristics and energy evolution law for varying lithologies, the loading was as much as 40% of the compressive material strength, which was subsequently unloaded. This was to model the hydraulic portal support's working principle. A loading speed of 0.2 mm/min was utilized. Uniaxial cycle loading adopted stress control. The cycle loading and loading rate was 0.1 MPa/s and there were four cycles. After the cycle loading, the loading continued until the specimen ruptured and experienced instability. The test process was completed in the ROCK600-50 rock test system according to the set control procedure. Figure 3 shows the ROCK600-50 rock test system. The cycle loading method is shown in Figure 4.

2.3. Results and Discussion

2.3.1. Basic Mechanical Properties. Table 2 contains an average for mechanical parameters for different lithological samples and the testing processes. One should note that after the

(a)

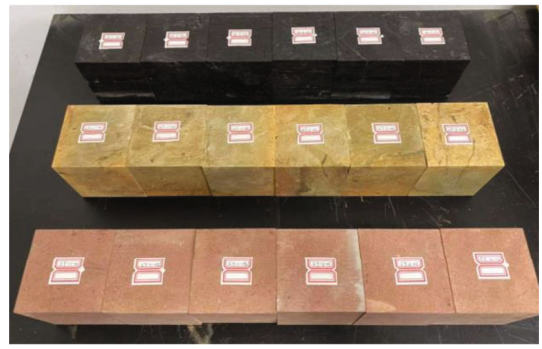

(b)

Figure 2: Processing instruments and produced rock samples. (a) Rock sample processing instrumentation and (b) resulting test sample.

Figure 3: ROCK600-50 testing system.

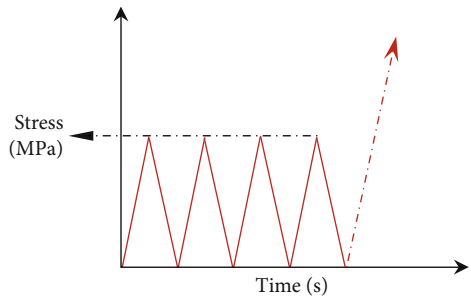

Figure 4: Cyclic loading mode. The compressive strength of rock sample is 40% and the loading/unloading slope is $k = \pm 0.1$ MPa/s.

cyclic loading, loading was continued until the specimen fractured and became unstable. The sandstone, mudstone, and coal strength limits decreased, with the coal strength limit decreased significantly by 15.42 MPa. At 40% cyclic loading and unloading, the average elastic modulus of mudstone and coal was greater than that of uniaxial compression. The sandstone elastic modulus was reduced but not significantly. The test indicated that the elastic modulus for the three rocks did not change significantly after four cycles of loading and unloading. The cyclical loading improved rock deformation resistance but produced defects within the fine visual structure inside the rock (such as microcracks and microholes). The above conclusions can be explained by examining the energy evolution and magnitude of rock damage.

2.3.2. Deformation Characteristics Analysis. During loading and unloading, elastic deformation and plastic deformation will continuously occur. The elastic deformation will be completely recovered after the removal of the stress, while the plastic deformation will accumulate and increase continuously during each cycle of loading and unloading. Such deformation is referred to as residual strain. Figure 5 shows the stress-strain curves of uniaxial compression and cyclic loading for different lithologies. Under cyclic loading, the stress-strain curves of different lithologies are similar to the uniaxial compression curves, which are divided into compaction, elastic, plastic, failure, and residual stages.

Each cycle produces plastic deformation, which results in a constant shift to the right for the hysteresis curve. Because the pore cracks in the initial cycle are not compacted by the test piece, the first residual strain generated by the initial cycle is larger than that of later cycles. The strain difference under different cycles and the residual strain difference are shown in Figure 6. The unrecoverable strain generated when the stress is unloaded is the residual

Table 2: Table of varying lithologic mechanical parameters.

	Lithology	The specimen number	Strength of limit (MPa)	Average intensity (MPa)	Modulus of elasticity (GPa)	Average elastic modulus (GPa)
Uniaxial compression	Sandstone	SY-1-01	58.58	56.04	4.173	3.861
		SY-1-02	52.48		3.490	
		SY-1-03	57.06		3.920	
	Mudstone	NY-1-01	12.29	10.89	1.099	0.981
		NY-1-02	9.24		0.704	
		NY-1-03	11.13		1.139	
	Coal	M-1-01	13.09	30.31	1.228	1.296
		M-1-02	32.33		1.420	
		M-1-03	28.29		1.241	
Cyclic loading and unloading	Sandstone	SY-2-01	55.39	50.34	3.582	3.665
		SY-2-02	45.29		3.748	
	Mudstone	NY-2-01	12.00	9.96	0.896	1.030
		NY-2-02	7.92		1.164	
	Coal	M-2-01	13.90	14.89	1.256	1.364
		M-2-02	15.87		1.472	

strain. However, in the stress-strain curve, with increasing stress, the difference between the two adjacent loading curves increases. This indicates that the corresponding strain difference at a given stress state is greater than the residual strain generated by a given cycle. This implies that some of the irreversible deformation under high stress is restored at low stress conditions. This portion of recoverable deformation may a result of the microelement rebound of rock, the recovery of microdefects, and other similar factors. This portion of the recoverable deformation may result in the illusion of large irreversible strain under a load threshold.

One may observe from the above data that the residual strain difference of the first coal cycle is larger than that of other lithologies, which indicates that there are many cracks and holes in the coal body resulting in large unrecoverable deformation. The sandstone interior itself contains comparatively fewer defects; consequently, the unrecoverable deformation is small. Mudstone has the lowest elastic modulus, low deformation resistance, significant deformation ability, and good recovery ability. Consequently, the residual deformation produced by the first cycle addition and unloading is less than other lithologies.

2.3.3. Analysis of Macrodestruction Characteristics. Three different lithological cubes loaded to fracture are shown in Figure 7. These specimens include three lithologies. The sandstone specimen shows principally tapered damage, and the mudstone specimen principally exhibits shear failure at angles of 45°. For the coal specimens, failure is generally tapered with some shear failure along angles of 45° along with split failure. For these fracture conditions, a theoretical study of 45° shear failure and cone failure is performed.

(1) Shear Failure. When the test block is in a state of uniaxial compressive stress, the mechanical model of the shear belt with a point of its force is shown in Figure 8. According to the mechanical model for the uniaxial stress state, the stresses along the oblique m-n plane are analyzed. The axial pressure is decomposed into components parallel, τ_n, and orthogonal to the m-n direction, σ_n. Using the Moore-Coulen criterion principle, the following formulas are obtained.

$$\sigma_n = \frac{1}{2}\sigma_1 + \frac{1}{2}\sigma_1 \cos 2\beta = \sigma_1 \cos^2\beta, \tag{1}$$

$$\tau_n = \frac{1}{2} \sin 2\beta = \sigma_1 \sin\beta \cos\beta. \tag{2}$$

Here, τ_n is the "sliding force" that causes shear damage, and σ_n improves the sliding friction resistance on the rupture surface. The value of the angle β affects the magnitude of τ_n and σ_n. The oblique section τ_n has the largest shear stress when β is 45°, but the shear resistance at the oblique section of 45° is the minimum. The surface generally ruptures at the section with the largest difference between the shear stress and the shear strength. The failures for the specimens with the three types of lithology generally occur on surfaces oriented at angles of 45° from the applied load.

According to the Moore-Coulen criterion, the shear strength τ_f at an angle β can be expressed as

$$\tau_f = c + \mu\sigma_n. \tag{3}$$

Here, c is the cohesive force (MPa), and μ is the friction coefficient on the inclined section, which is related to the roughness of the inclined section. $\mu = \tan\varphi$, where φ is the internal friction angle of the rock sample.

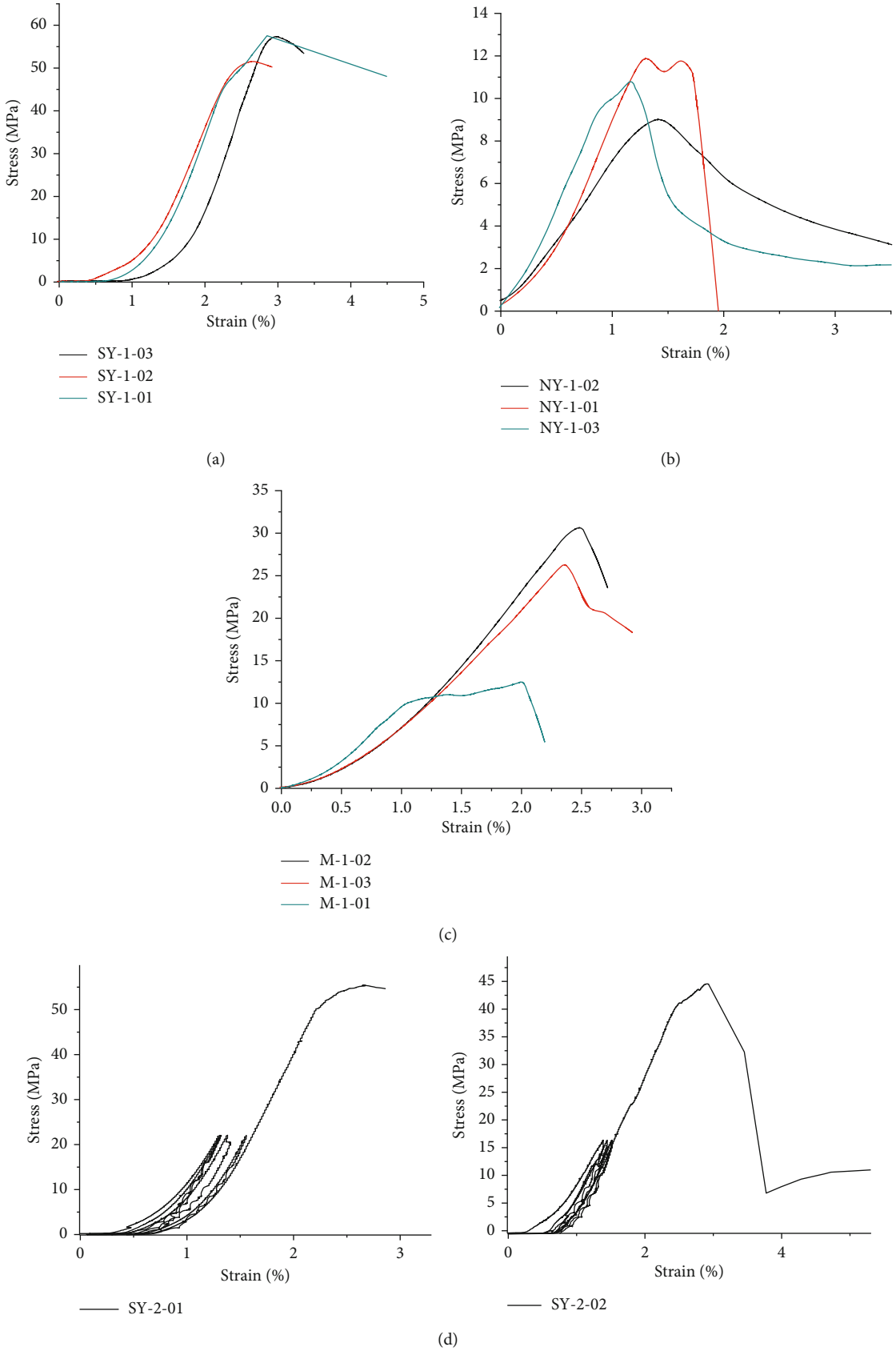

Figure 5: Continued.

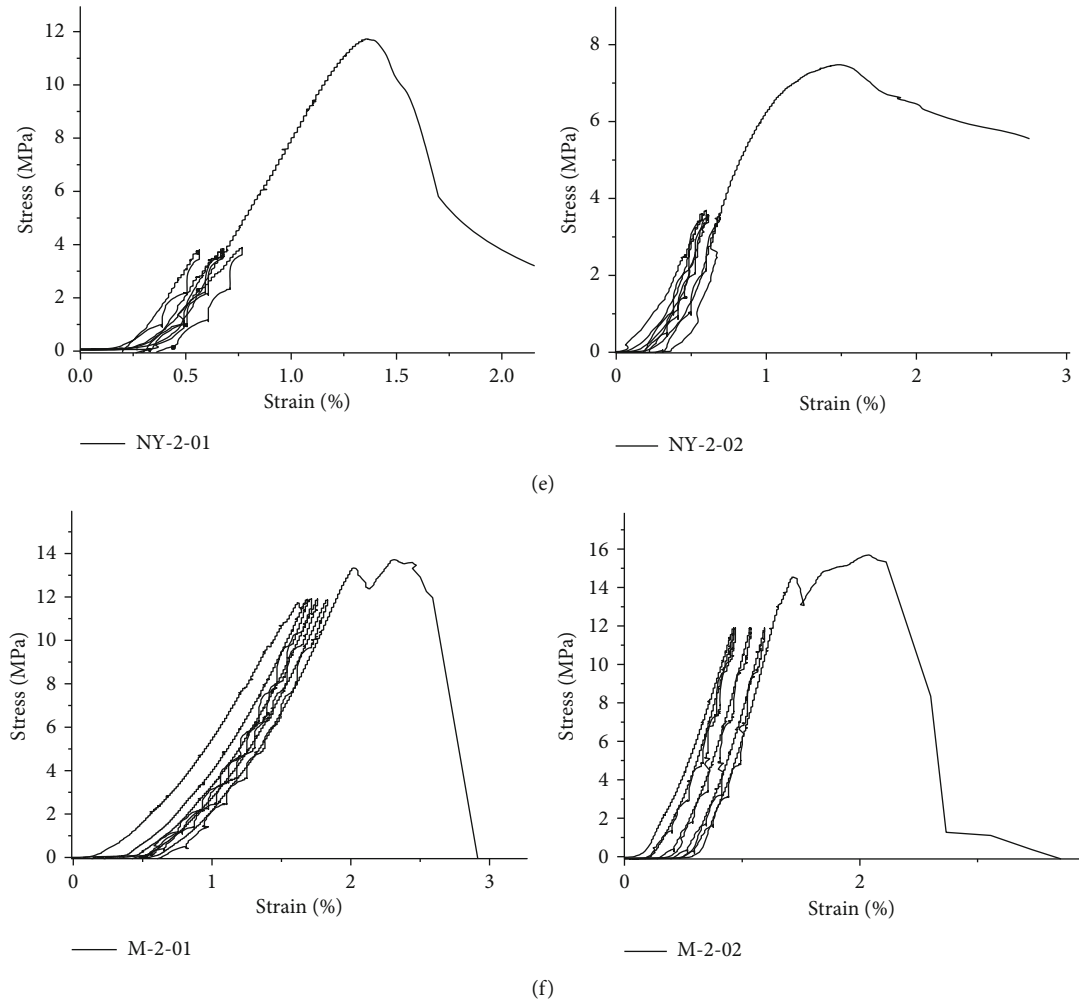

Figure 5: Total stress-strain curves. (a) Uniaxial compression for the SY lithology. (b) Uniaxial compression for the NY lithology. (c) Uniaxial compression for the M lithology. (d) Cyclic loading for the SY lithology. (e) Cyclic loading for the NY lithology. (f) Cyclic loading for the M lithology.

When the coaxial pressure is greater than a threshold value, the shear stress, τ_n, exceeds the shear strength τ_f, and fracture occurs along the oblique β surface. The oblique β cross section is the most probable rupture surface with the rock sample. The equation for τ_n at oblique angle β at the limit of instability balance is

$$\tau_n \geq \tau_n = c + \mu\sigma_n. \tag{4}$$

Substituting equations (1) and (2) into equation (4) yields

$$\frac{1}{2}\sigma_1 \sin 2\beta \geq c + \mu\sigma_1 \cos^2\beta. \tag{5}$$

One may observe that shear damage occurs under the conditions indicated previously. In addition, provided the strength parameters for lithology, c, μ, and σ_1, are known, the rupture angle range and the most probable fracture angle can be utilized to mitigate fraction risk.

(2) Cone Destruction. The cone disruption is caused by the end-surface effect and shear. The test machine places pressure on the sample face oriented toward the end face's center of the friction. Consequently, the transverse deformation of the sample face is constrained, which restricts the lateral deformation of the test sample and has a role similar to the peripheral pressure. In the process of sample transition from plastic deformation to fracture, specimen expansion becomes more significant. The end surface effect has a more important role as the loading continues. Friction with the rigid loading plate restricts movement to two specimen sides. Farther from the upper and lower specimen surfaces, where the friction effect is less, the largest lateral displacement occurs. This is approximately near the middle of the rock sample. The observed and calculated damage agree well near the middle of the outward bulge, which is shown in Figure 9.

Prior to fracture, the specimen "collapse zone" (near the specimen exterior at axal locations close the maximum deformation) generally fractures and falls from the sample.

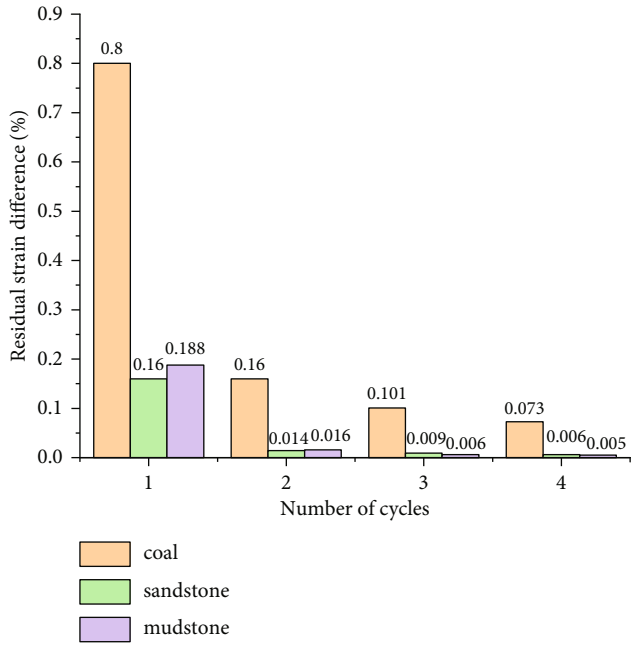

Figure 6: Residual strain difference of different lithologies with number of cycles.

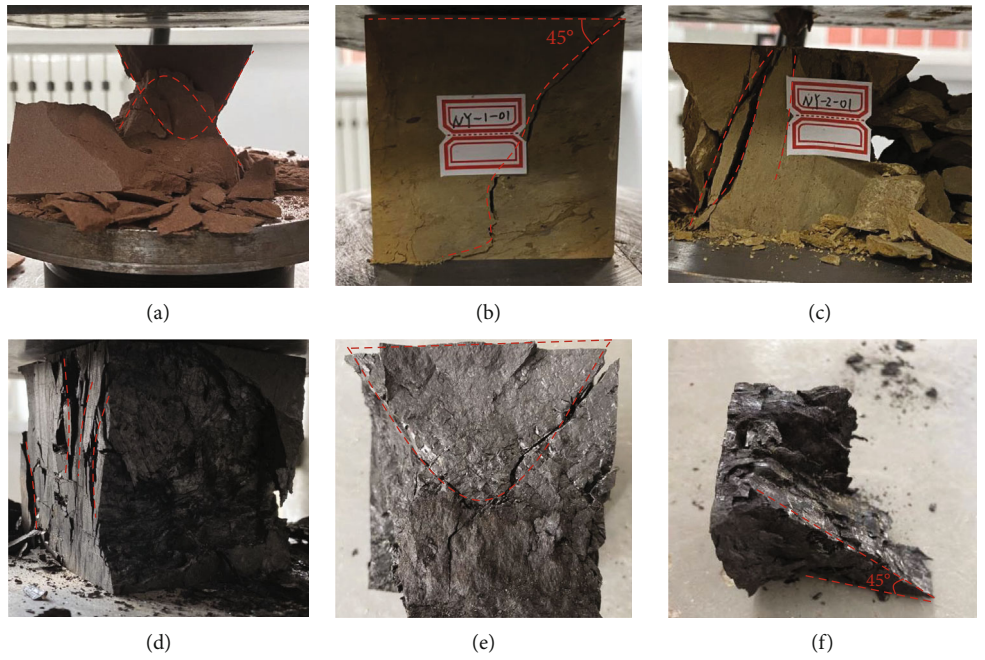

Figure 7: Typical fracture patterns for different lithological specimens. (a) Sandstone (cone damage). (b) Mudstone (45° shear damage). (c) Mudstone (crack break). (d) Coal (split break). (e) Coal (tapered damage). (f) Coal (45° shear damage).

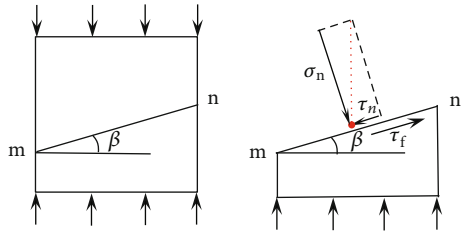

Figure 8: Stress components during axial loading.

The "thrust area" (areas of the sample influenced by the deformation constraints introduced by loading) thrust zone has a tendency to penetrate into the cube. With increasing pressure, two intersecting shear planes are formed inside the rock sample. With increased loading, the thrust zone is crushed into the collapse zone. The outer surface begins to collapse. Finally, a pair of "core," damaged surfaces, which are approximately symmetric, results from the loading. This process is summarized in Figure 10.

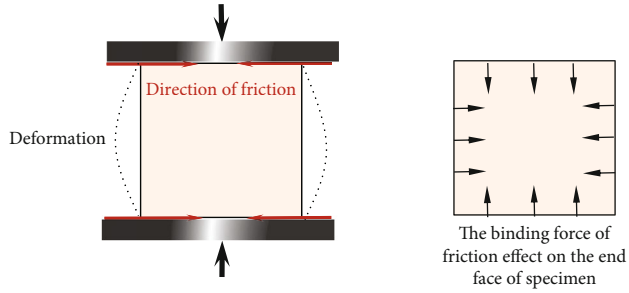

Figure 9: Deformation produced by friction at the specimen top and bottom faces.

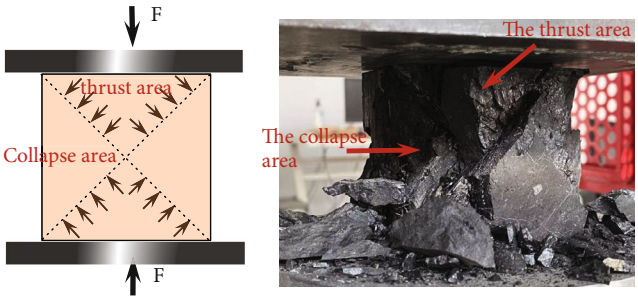

Figure 10: Shear slip surface under upper and lower constraints.

(3) Cleavage Breakdown. The mudstone and coal specimens showed cleavage failure. The probability of cleavage failure for mudstone was greater than that of coal, while sandstone did not show cleavage failure. The nature of splitting failure is that the rock tensile strength is significantly less than the compressive strength, and the mudstone and coal specimens reach their tensile strength before reaching their compressive strength. This resulted in tensile cracks within the rock samples. Under cyclic loading, tensile cracks grew and eventually formed splitting failure surfaces. The compressive strength of the three lithologies was in the order sandstone > coal > mudstone. The sandstone specimen's compressive strength was much greater than that of coal or mudstone. Specimens with small compressive strength were subjected to small compressive pressure by the pressing plate. Regarding the neglecting of the end faces' friction coefficient, the friction effect of the end face can be reduced by using a specimen with low compressive strength. This low compressive strength was also a reason for the specimen splitting failure.

(4) Energy Analysis and Rock Damage under Cycle Loading and Unloading. Rock damage is a deterioration process of material or structure caused by fine structure defects (such as microcracks and microholes), under the action of external loading and environmental factors. Energy is the driving force driving the development of fine structural defects; consequently, the rock deformation and fracture processes must be accompanied by capacity transformation. It is feasible to analyze the energy transformation characteristics of the rock deformation and rupture process to characterize the magnitude of rock damage.

The process of rock cycle loading and unloading results in the external force constantly performing work on the specimen. The external force is converted into elastic strain and dissipation energy. Using the principles of thermodynamics, energy transformation is the essential process by which the energy state of the specimen changes, as manifested by the rock deformation. Ultimately, the destruction of the specimen is an instability driven by changes of internal energy. According to the conservation of energy,

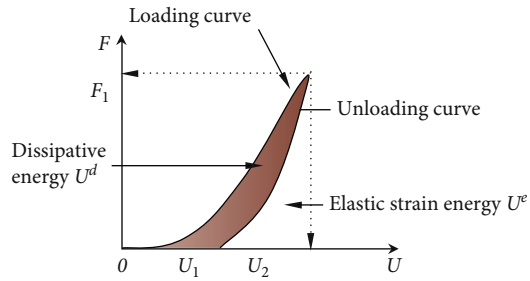

Figure 11: Calculated areas and the interrelationship of elastic strain energy and dissipation energy.

$$U = U^e + U^d. \tag{6}$$

Here, U is pressure performing work on the rock, specifically, the strain energy stored within the rock lattice. U^d is the dissipative energy transferred to the rock's lattice during the loading process. U^e is the elastic strain energy transferred to the rock's lattice during the loading process.

During rock loading, a portion of the transferred energy is absorbed by the rock's lattice is consumed to drive plastic deformation and damage, such as the formation and development of cracks. The other portion of transferred energy is stored in the lattice rock as elastic strain energy. This energy is completely recovered when the rock sample is unloaded. In cyclic loading, the elastic strain energy and dissipation energy are numerically equal to the area enclosed by the corresponding full stress-strain curve and the coordinate axis, as shown in Figure 11.

Based on basic principles and methods of energy analysis, cumulative dissipated energy is proposed to be indicative of energy dissipation after different cycles. The magnitude of damage is defined as the ratio of cumulative total strain energy to that at the cycle of specimen failure. The calculation of cumulative dissipated energy is shown in equations (7)–(9). The full stress-strain curve data of different lithology cube specimens were decomposed, and the area of each cycle was calculated by using the integral function provided in Origin software.

$$U^d(i) = \sum_{k=1}^{i} U_k^d, \tag{7}$$

where $U^d(i)$ is the cumulative dissipated energy in cycle i and U_k^d is the dissipated energy during cycle k.

$$U(i) = U^e(i) + U^d(i), \tag{8}$$

Table 3: Changes of various energy parameters for cycle loading and unloading.

(a)

Lithology	Coal			
Number of loading and unloading cycles	Cumulative dissipation energy U^d (kJ·m^{-3})	Cumulative strain energy U (kJ·m^{-3})	Degree of damage D (%)	Mean degree of damage (%)
1	1.016	4.098	3.16	3.23
	0.982	4.048	3.30	
2	1.949	7.549	6.06	6.26
	1.923	7.392	6.45	
3	2.740	10.973	8.52	8.86
	2.741	10.689	9.20	
4	3.356	14.335	10.44	10.85
	3.352	14.062	11.25	
The final cycle		32.156	100.00	
		29.799		

(b)

Lithology	Mudstone			
Number of loading and unloading cycles	Cumulative dissipation energy U^d (kJ·m^{-3})	Cumulative strain energy U (kJ·m^{-3})	Degree of damage D (%)	Mean degree of damage (%)
1	0.720	1.088	3.36	3.21
	0.590	1.326	3.05	
2	1.055	1.877	4.93	4.78
	0.892	2.503	4.62	
3	1.451	2.684	6.78	6.53
	1.211	3.744	6.27	
4	1.935	3.624	9.04	8.45
	1.519	4.974	7.86	
The final cycle		21.40	100	
		19.32		

(c)

Lithology	Sandstone			
Number of loading and unloading cycles	Cumulative dissipation energy U^d (kJ·m^{-3})	Cumulative strain energy U (kJ·m^{-3})	Degree of damage D (%)	Mean degree of damage (%)
1	2.261	7.730	1.71	2.10
	3.314	7.269	2.48	
2	3.663	14.919	2.76	3.18
	4.810	12.681	3.60	
3	5.791	21.787	4.37	4.93
	7.312	19.338	5.48	
4	6.629	28.809	5.00	6.17
	9.788	26.047	7.33	
The final cycle		132.539	100.00	
		133.449		

where $U(i)$ is the cumulative total strain energy during cycle i and $U^e(i)$ is the cumulative elastic strain energy during cycle i.

$$D(i) = \frac{U^d(i)}{U(t)} * 100\%, \tag{9}$$

where $D(i)$ is the magnitude of rock damage when loading to cycle i and $U(t)$ is the cumulative total strain energy at the failure cycle.

After the conversion of the strain, the test results are shown in Table 3.

Based on test data, the cumulative energy dissipation and rock damage trends are shown in Figure 12.

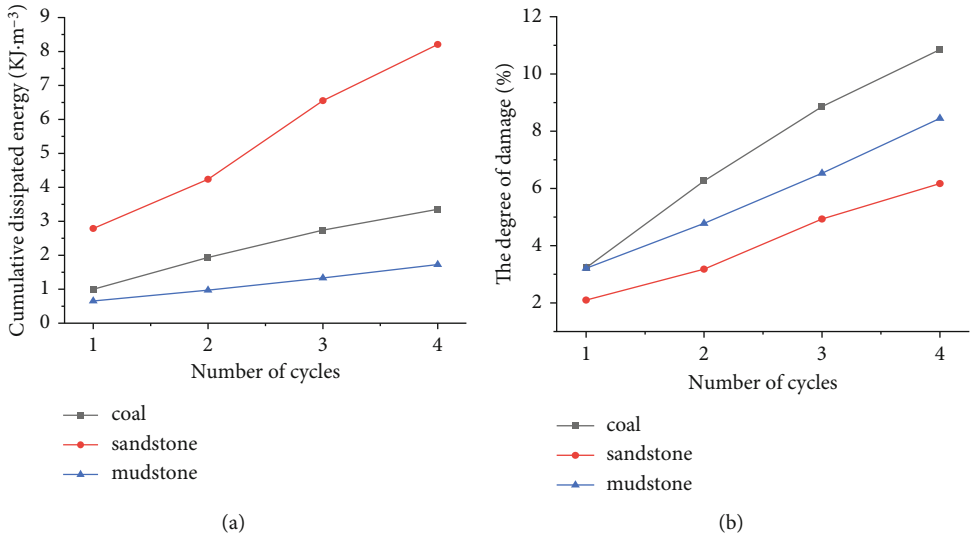

Figure 12: (a) Average cumulative dissipated energy. (b) Average degree of rock damage.

Figure 13: (a) Uniaxial compression failure state. (b) Cyclical loading final failure state.

Using the data presented, one can arrive at the following conclusions. First, compared with the other two lithologies, sandstone has the highest cumulative dissipation energy, but after four loading cycles, its damage is the lowest at only 6.17%. This reflects the property of sandstone to have superior antifatigue ability compared with that of coal and mudstone. Second, the cumulative dissipated energy of coal is inferior to that of sandstone, but the magnitude of damage for coal is the highest of the studied lithologies. After four loading cycles, the damage is 10.85%. This conforms with its deformation characteristics, and the strength limit of coal decreases the most of the considered lithologies, with a decrease of 15.42 MPa. The deformation characteristics and energy and magnitude damage verify each other. This infers that the test results are reasonable. Third, for mudstone, the cumulative dissipation energy after four loading cycles is the minimum of the considered lithologies. This indicates significant elastic deformation for mudstone in addition to a significant internal deformation energy of total strain energy. This results in low energy dissipation, which is similar to the low residual strain of mudstone. Fourth, under different lithological cycle loading modes, loud sounds were emitted during rock damage. This was accompanied by the ejection of rock debris. The sandstone absorbs the most energy of the considered lithologies. It stores the most elastic strain energy, and the rupture magnitude is greater than other considered lithologies.

During the test procedure, both coal and sandstone suffered burst damage when the uniaxial compression reached the ultimate compressive strength. The damaged area, fragmentation, and fragment speed were all "violent" than the state caused by cyclic loading. This was mainly due to the energy evolution difference between uniaxial compression and cyclic loading. This is shown in Figure 13 for sandstone.

The observed behavior, including magnitude of damage, of different rocks can be explained by the energy evolution process. Studies have explained the principal reasons for rock damage using energy conversion. Any rock stress state corresponds to an energy state, from elastic and plastic deformation to failure. Energy is always exchanged with the surroundings, to maintain dynamic balance. Before the rock mass reaches the ultimate stress, it primarily absorbs energy from the surroundings. After the rock reaches the ultimate stress, it releases this energy back to the surroundings. The dynamic failure of rock is the result of the rapid

accumulation and release of internal elastic energy in the failure state. For the coal and sandstone, which exhibited significant burst damage, the cyclic loading and magnitude fracture can be analyzed from the perspective of energy conservation. The same analysis can be performed for fragment ejection velocity being less than that of uniaxial compression. With an increasing of the number of loading cycles, the dissipative energy accumulated continuously, promoting the continuous formation and development of cracks. Finally, through theoretical calculation, the magnitude of damage for of coal and sandstone were 10.85% and 6.17%, respectively. This indicated that these rock samples were in the "plastic state." When the rock sample reached the ultimate strength failure, the elastic strain energy released by instantaneous unloading was less for the cyclic loading than for simple uniaxial loading.

3. Conclusions

It was demonstrated that the modulus of elasticity of the three lithologies did not change significantly after four loading cycles. The loading cycles improved the rock's antideformation ability but caused material defects (such as microcracks and microvoids) in the internal rock mesostructure. The magnitude of damage degree was the greatest for coal. It was also found that the ultimate strength decreased the most for coal, decreasing by 15.42 MPa. The magnitude of damage degree calculated by theory is consistent with the mechanical properties observed in the test.

There are many defects, such as fissures and holes, with in the coal body. This resulted in large, unrecoverable deformation. Mudstone had the smallest elastic modulus, but it had significant deformation and recovery ability; consequently, the residual deformation produced by the first cyclic loading was small. Comparing the failure modes of the three cubic lithologies, except the mudstone and coal specimens which generally failed by splitting failure, the specimens generally failed by shear and conical failure.

Under the same lithology and different loading modes, rock damage was caused by cyclic action, and energy evolution was different between the specimens. The transient unloading with significant previous damage may release less elastic strain energy. The cyclic loading and had a smaller fracture damage than that of uniaxial compression. Under different cyclic loading modes for different lithologies, sandstone absorbed the most energy, stored the most elastic strain energy, and had the largest magnitude of rupture destruction compared to other lithologies.

Data Availability

The data used to support the findings of this study are available from the corresponding author upon request.

Conflicts of Interest

The authors declare no conflicts of interest.

Acknowledgments

This study was sponsored by the Shandong Provincial Key R&D Plan of China (Grant No. 2019SDZY034-1), the Engineering Laboratory of Deep Mine Rock Burst Disaster Assessment Open Project (LMYK2020007), and the National Natural Science Foundation of China (Grant Nos. 51504145 and 51804182). The authors are grateful for their support.

References

[1] H. P. Xie, F. Gao, Y. Ju et al., "Quantitative definition and investigation of deep mining[J]," *Journal of China Coal Society*, vol. 40, no. 1, pp. 1–10, 2015.

[2] K. Hongpu, "Stress distribution characteristics and strata control technology for roadways in deep coal mines[J]," vol. 41, no. 9, pp. 12–17, 2013.

[3] L. Fuqiang, Q. Guangpeng, L. Yonggang, W. Qichen, W. Ying, and H. Fengjun, "Study on the mechanism of gas ignition by friction effect of hard quartz sandstone instability," *Geofluids*, vol. 2020, 17 pages, 2020.

[4] H. P. Xie, F. Gao, and Y. Ju, "Research and development of rock mechanics in deep ground engineering[J]," *Chinese Journal of Rock Mechanics and Engineering*, vol. 34, no. 11, pp. 2161–2178, 2015.

[5] C. Meifeng, H. Manchao, and L. Dongyan, *Rock Mechanics and Engineering[M]*, Science Press, Beijing, 2012.

[6] T. Li, X. Pei, D. Wang, R. Huang, and H. Tang, "Nonlinear behavior and damage model for fractured rock under cyclic loading based on energy dissipation principle," *Engineering Fracture Mechanics*, vol. 206, pp. 330–341, 2019.

[7] Z. Wu, X. Ji, Q. Liu, and L. Fan, "Study of microstructure effect on the nonlinear mechanical behavior and failure process of rock using an image-based-FDEM model," *Computers and Geotechnics*, vol. 121, p. 103480, 2020.

[8] D. Lei, H. Lin, and Y. Wang, "Damage characteristics of shear strength of joints under freeze–thaw cycles," *Archive of Applied Mechanics*, vol. 92, no. 5, pp. 1615–1631, 2022.

[9] X. I. E. Kai-Nan, D. Y. Jiang, and J. I. A. N. G. Xiang, "Energy distribution and criticality characteristics analysis of shale Brazilian splitting test[J]," *Journal of China Coal Society*, vol. 42, no. 3, pp. 613–620, 2017.

[10] J. Yao and Z. Wang, "Mechanical behavior and damage evolution for granite subjected to cyclic loading," *Huashan granite[J].Hydro-Science and Engineering*, vol. 2018, pp. 1–10, 2018.

[11] Y. Y. Li, S. C. Zhang, Z. J. Wen et al., "Energy conversion and fragment distribution characteristics of coal sample under uniaxial cyclic loading[J]," *Journal of China Coal Society*, vol. 44, no. 5, pp. 1411–1420, 2019.

[12] W. Ping, Z. Yongjian, F. Tao, and Y. Weijian, "Test and analysis of sandstone damage-weakening under loading-unloading-loading[J]," *Journal of China Coal Society*, vol. 41, no. 12, pp. 2960–2967, 2016.

[13] Q. B. Meng, L. J. Han, H. Pu, S. Y. Wen, H. Li, and H. Li, "Experimental on the effect of strain rate and size on the energy accumulation and dissipation of rock[J]," *Journal of China Coal Society*, vol. 40, no. 10, pp. 2386–2398, 2015.

[14] J. F. Liu, J. Xu, Q. S. Li, and G. L. Li, "Experimental research on damping parameters of rock under cyclic loading[J]," *Chinese Journal of Rock Mechanics and Engineering*, vol. 29, no. 5, pp. 1036–1041, 2010.

[15] J. Xu, Y. Zhang, H. W. Yang, and J. N. Wang, "Energy evolution law of deformation and damage of sandstone under cyclic pore water pressures[J]," *Chinese Journal of Rock Mechanics and Engineering*, vol. 30, no. 1, pp. 141–148, 2011.

[16] Z. Zhizhen and G. Feng, "Research on nonlinear characteristics of rock energy evolution under uniaxial compression[J]," *Chinese Journal of Rock Mechanics and Engineering*, vol. 31, no. 6, pp. 1198–1207, 2012.

[17] L. Y. Li, Y. Ju, Z. W. Zhao, L. Wang, J. F. Lu, and X. Ma, "Energy analysis of rock structure under static and dynamic loading conditions[J]," *Journal of China Coal Society*, vol. 34, no. 6, pp. 737–740, 2009.

[18] H. Guo, M. Ji, D. Liu, M. Liu, and W. Zhao, "The influence of fracture strain energy on the burst tendency of coal seams and field application," *Advances in Civil Engineering*, vol. 2021, 10 pages, 2021.

[19] L. Yang, F. Q. Gao, X. Q. Wang, and J. Z. Li, "Energy evolution law and failure mechanism of coal-rock combined specimen[J]," *Journal of China Coal Society*, vol. 44, no. 12, pp. 3894–3902, 2019.

[20] Y. Liu, F. Dai, L. Dong, N. Xu, and P. Feng, "Experimental investigation on the fatigue mechanical properties of intermittently jointed rock models under cyclic uniaxial compression with different loading parameters," *Rock Mechanics and Rock Engineering*, vol. 51, no. 1, pp. 47–68, 2018.

[21] C. H. E. N. G. Cheng and L. I. Xiao, "Cyclic experimental studies on damage evolution behaviors of shale dependent on structural orientations and confining pressures," *Energies*, vol. 11, no. 1, p. 160, 2018.

[22] Y. Zhang, X. T. Feng, C. Yang, X. Zhang, M. Sharifzadeh, and Z. Wang, "Fracturing evolution analysis of Beishan granite under true triaxial compression based on acoustic emission and strain energy," *International Journal of Rock Mechanics and Mining Sciences*, vol. 117, pp. 150–161, 2019.

[23] Y. Zhang, X. T. Feng, X. Zhang, Z. Wang, M. Sharifzadeh, and C. Yang, "A novel application of strain energy for fracturing process analysis of hard rock under true triaxial compression," *Rock Mechanics and Rock Engineering*, vol. 52, no. 11, pp. 4257–4272, 2019.

[24] Z. H. A. O. Chuang, W. U. Ke, L. I. Shu-cai, and Z. Jiangang, "Energy characteristics and damage deformation of rock subjected to cyclic loading[J]," *Chinese Journal of Geotechnical Engineering*, vol. 35, no. 5, pp. 890–896, 2013.

[25] X. B. Yang, Y. P. Qin, and F. Ye, "Damage constitutive relation of sandstone considering residual stress[J]," *Journal of China Coal Society*, vol. 40, no. 12, pp. 2807–2811, 2015.

[26] Y. Zhao, L. Chang, Y. Wang, H. Lin, J. Liao, and Q. Liu, "Dynamic response of cylindrical thick-walled granite specimen with clay infilling subjected to dynamic loading," *Archive of Applied Mechanics*, vol. 92, no. 3, pp. 643–648, 2022.

[27] X. Fan, H. Yu, Z. Deng, Z. He, and Y. Zhao, "Cracking and deformation of cuboidal sandstone with a single nonpenetrating flaw under uniaxial compression," *Theoretical and Applied Fracture Mechanics*, vol. 119, p. 103284, 2022.